

Supervised Classification and Lineaments Extraction of SPOT-5 Imageries in the Geological Mapping of Kutaina–Al Hajar Area, Arabian Shield, Saudi Arabia

Adel Zein Bishta, Abdullah Rasheed Sonbul

Faculty of Earth Sciences, King Abdulaziz University

Telephone: +966530911301; Emails: abishta@kau.edu.sa or adel_zein2@yahoo.com

Abstract: Supervised classification and lineaments extraction techniques were applied to the SPOT-5 data for the geological mapping of Kutaina–Al Hajar area of the Asir terrane in the southern part of the Arabian Shield, Saudi Arabia. The area under study has mainly N-S trending metamorphic and Metasediments belts. These rocks are hosted economic mineralization such as gold and copper, located at Kutaina mine in the north and Al Hajar mine in the south. The metamorphic rocks are emplaced by different plutonic intrusions of primarily diorite, syenite and porphyry granite bodies. This study aims to using the image processing techniques for the geological mapping and determine the factors controlled the mineralized alteration zones of the investigated area. SPOT-5 Multispectral data and the interpretation of the constructed color composite SPOT image and the field verification produced a detailed geological map, of Kutaina–Al Hajar area in scale 1:20,000.

[Adel Zein Bishta, Abdullah Rasheed Sonbul. **Supervised Classification and Lineaments Extraction of SPOT-5 Imageries in the Geological Mapping of Kutaina-Al Hajar Area, Arabian Shield, Saudi Arabia.** *Life Sci J* 2015;12(11):80-92]. (ISSN:1097-8135). <http://www.lifesciencesite.com>. 9.

Keywords: Supervised classification; lineaments extraction; alteration zones; Arabian Shield, Kutaina mine; Al Hajar gold mine

1. Introduction

Kutaina-Al Hajar area is located in the northwestern portion of the Asir terrane, Arabian Shield, approximately 80 km southeast of Al-Aqiq City. It is located between latitudes 19° 56' to 20° 10' N and longitudes 41° 55' to 42° 07' E (Fig. 1). This area is composed essentially of metasediments, metavolcanics and some intrusive igneous bodies of Precambrian age. The Arabian Shield comprises five major tectonic terranes: Asir, Al Hijaz, Madyan, Afif, and Ar Rayn. The first three terranes are formed of an intraoceanic island arc, and they are located at the western part of the Shield. The other two are of continental origin and are located on the eastern part of the Shield. These tectonic terranes are separated by four suture zones that are decorated by ophiolite belts. The sutures include Bir Umq, Yanbu, Nabitah, and Al-Amar (Al-Shanti, 2009). Bamousa (2013) studied the late Proterozoic rocks of the Mount Ablah mining prospect to the west of the study area.

Kutaina-Al Hajar area has not been previously subjected to detailed geological studies. Reconnaissance geological mapping of the study area was conducted within the regional map of the Al Aqiq Quadrangle on the scale of 1:100,000 by Greenwood in 1975. Many authors applied the image processing techniques for the geological mapping such as: Abrams, et al., 1983; Davis and Berlin, 1989; Sultan et al., 1986; Sultan et al., 1987; Gibson and Power, 2000; Madany and Bishta, 2002; Gupta, 2003; Bishta, 2004; Jutz, and Chorowicz, 1993; Lillesand et al., 2004; Wielen et al., 2004; Kavak and Cetin, 2007;

Bishta, 2008; Amer et al., 2009; Bishta, 2010; Sabins, 1999; El Janati et al., 2013; Guha et al., 2014. Antonielli et al., (2009) used remote sensing optical images that were integrated with ancillary data and ground truth information for the detailed mapping of the volcano-sedimentary succession of the Lower Dogali Formation in NE Aritrea. Haselwimmer et al. (2010) classified granitoid intrusive rocks and altered rhyolitic volcanic rocks of eastern Adelaide Island using the spectral properties of the ASTER data. This work aimed mainly to apply supervised classification of the digital SPOT-5 data for the geological mapping of the investigated area. This study also extend to determine the factors controlled the alteration zones bearing mineralizations (Blenkinsop, 2014, Doyle et al., 2013).

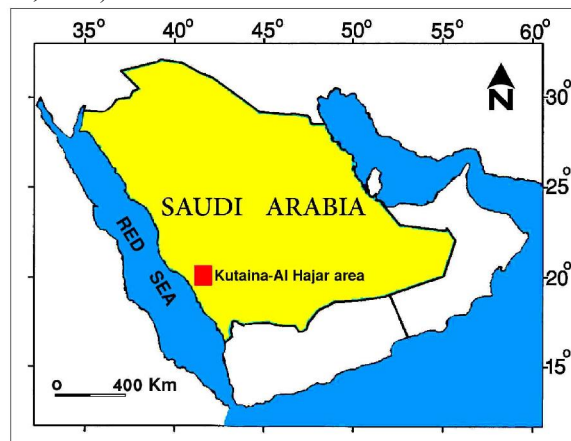


Figure 1. Location map of the study area

2. Methodology

The unsupervised and supervised classification methods are used in this work to discriminate the different lithologic units and trace the major structural lineaments of the study area.

Two main types of digital satellite imageries are used: Landsat-7 Enhanced Thematic Mapper plus (ETM+) data, and SPOT-5 data. The remotely sensed raw data of the study area are included in the Landsat-7 data with a scene number of path/raw = 175/40, and in the SPOT-5 data, the scene number is path/raw = 139/310. The visible, near-infrared and short wave infrared bands of the Enhanced Thematic Mapper ETM+ data are also processed.

The Landsat ETM+ data consist of 7 bands. The infrared ETM+ bands were characterized by the wavelength intervals of 760 to 900 nm (band 4), 1500 to 1750 nm (band 5) and 2080 to 2350 nm (band 7). The visible ETM+ bands, 1, 2 and 3, were characterized by wavelength intervals of 450 to 520 nm for band 1, 520 to 600 nm for band 2 and 630 to

690 nm for band 3. The Landsat ETM+ imagery data were characterized by a spatial resolution of 30 m (multispectral bands 1, 2, 3, 4, 5 & 7), 60 m (thermal band 6) and 15 m (panchromatic band 8).

The supplementary data that covers the study area includes geological maps of the previous work and the topographic maps on a scale of 1:50,000. The topographic maps were used in the processing of the geometric corrections of the Landsat ETM+ and SPOT-5 data.

The SPOT-5 data comprises 5 bands; the visible bands are characterized by wavelength intervals of 500 to 590 nm (band 1) and 610 to 680 nm (band 2) and near infrared bands from 780 to 890 nm (band 3). The short wave infrared band has wavelength intervals of 1580 to 1750 (band 4). The panchromatic band was characterized by wavelength intervals of 480 to 710 nm (band 5). The satellite imagery of the SPOT-5 data is characterized by a spatial resolution of 10 m (multispectral bands 1, 2, 3), 20 m (SWIR band 4) and 2.5 m (panchromatic band 5).

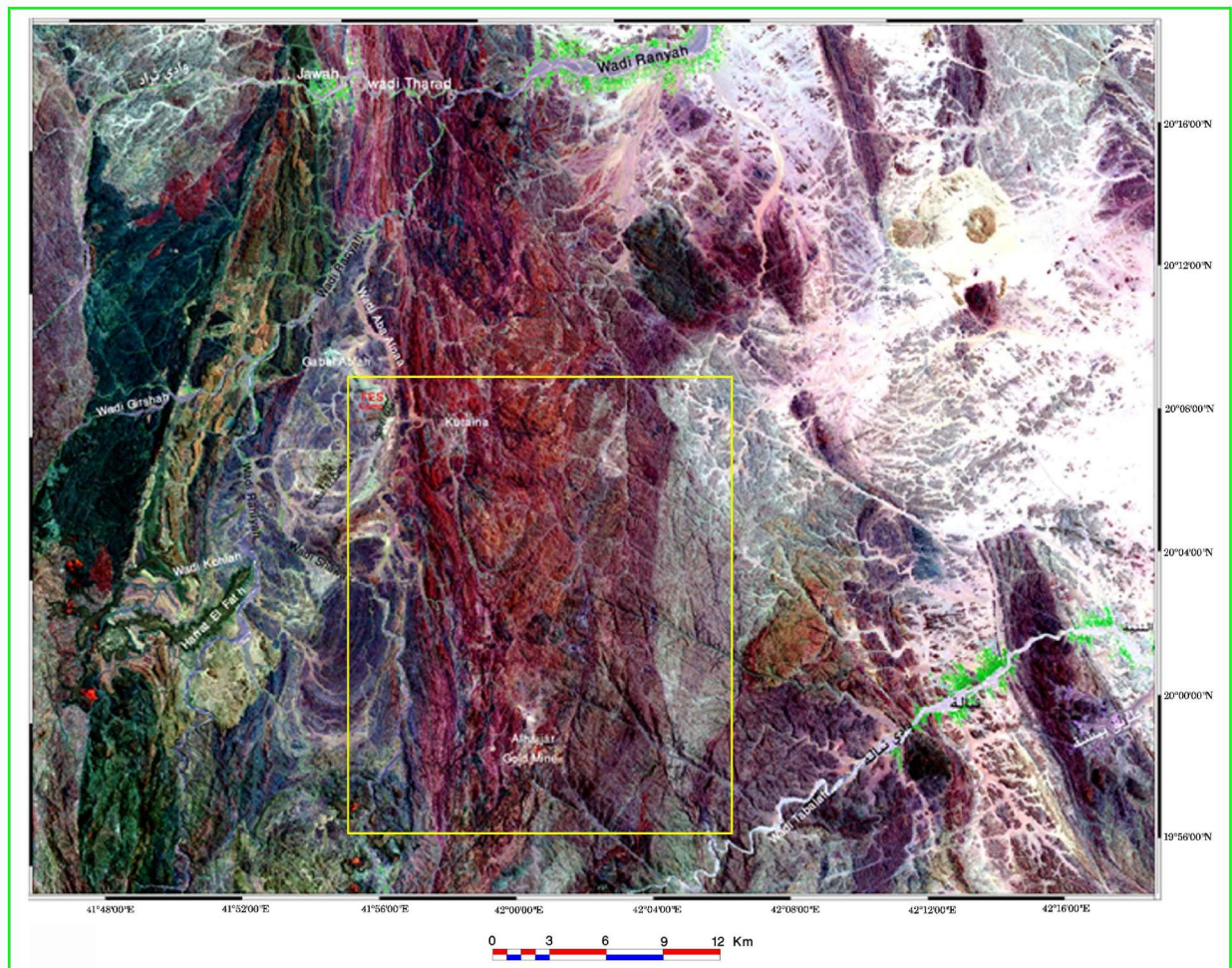


Figure 2. False color composite Landsat image, ETM+ bands 7, 4, 2 in RGB, showing the Kutaina–Al Hajar area in the yellow square (Original scale 1:100,000)

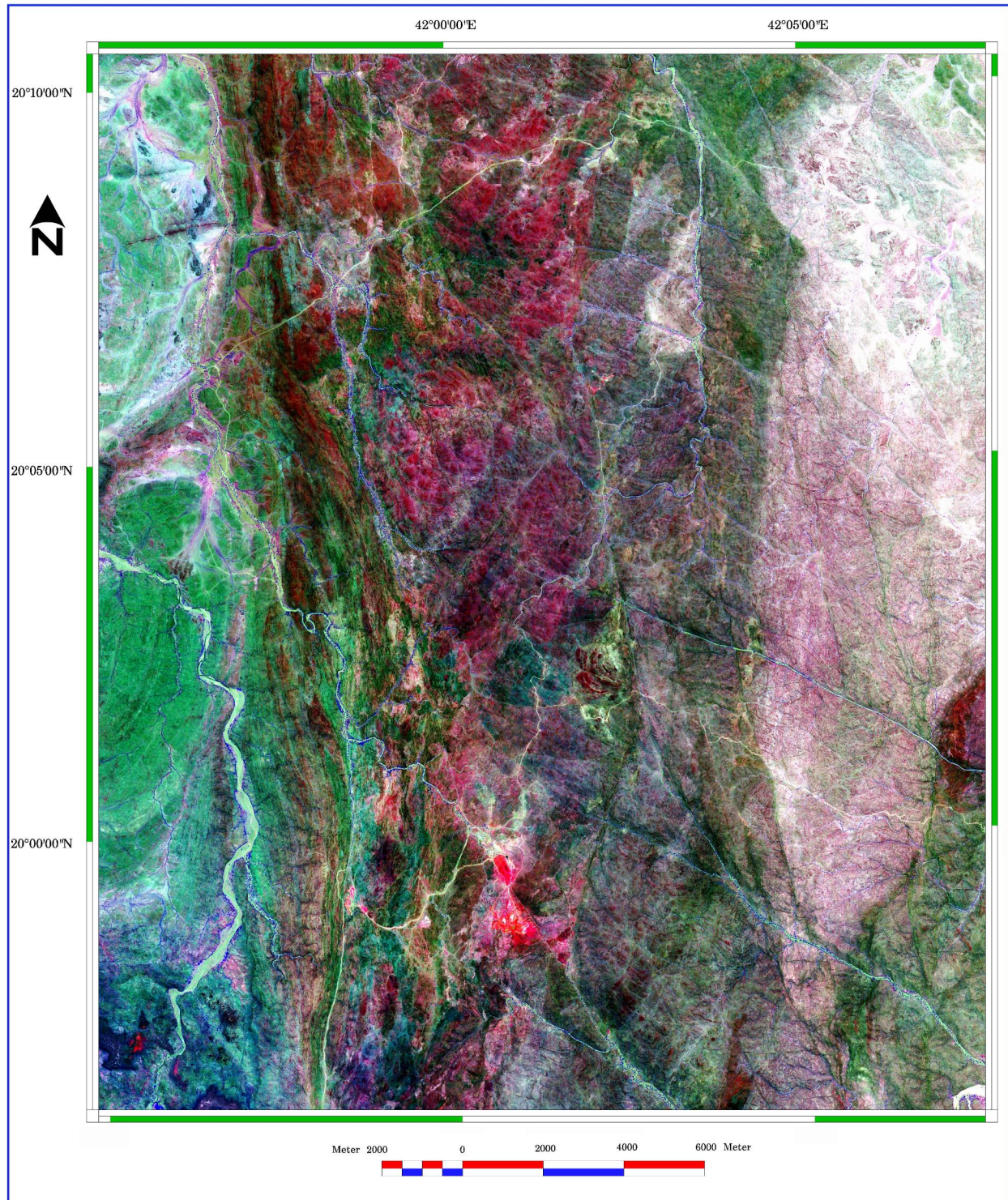


Figure 3. False color composite SPOT image of Kutaina–Al Hajar area, bands 4, 3, 1 in RGB (Original scale 1:20,000)

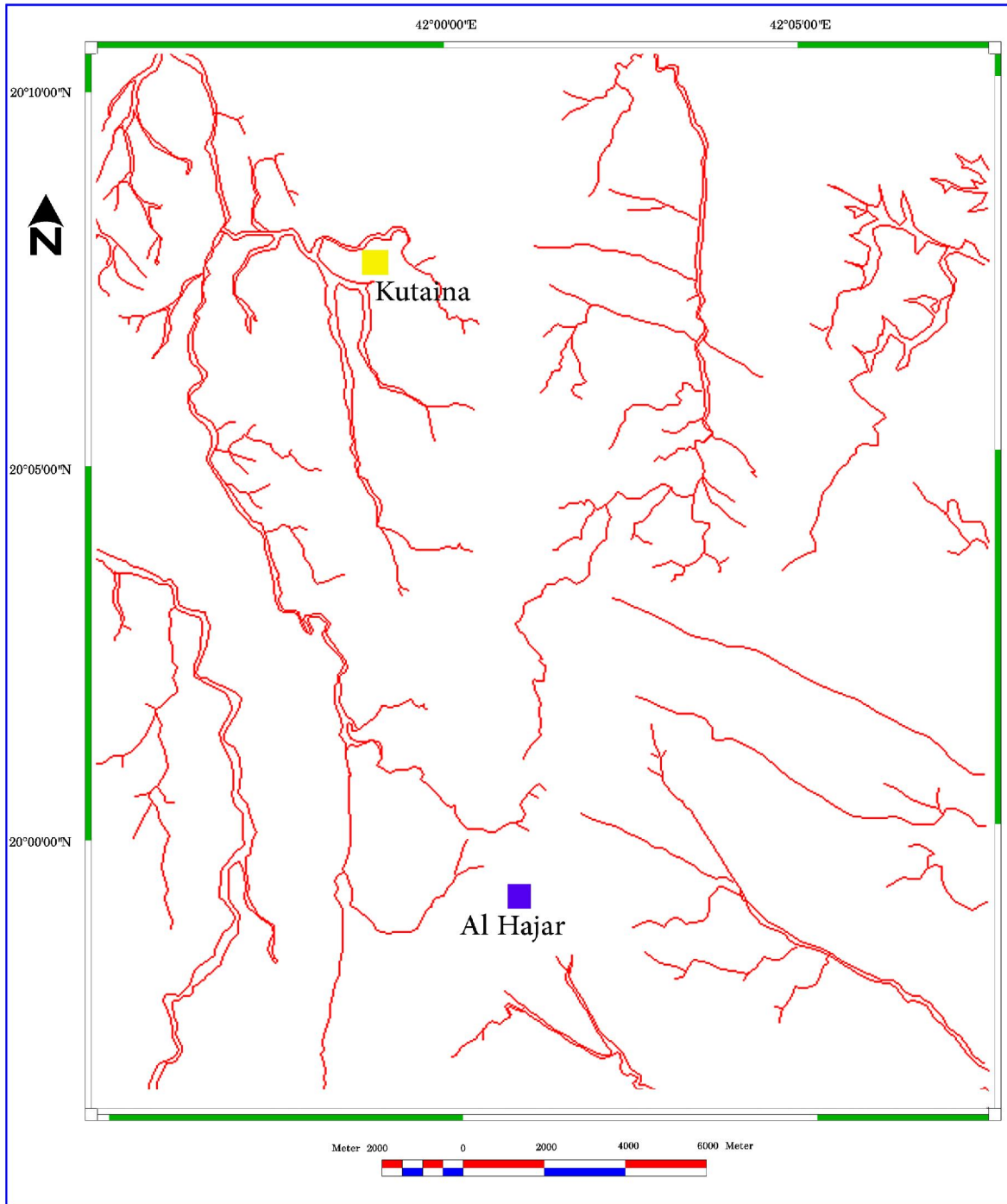


Figure 4. Drainage patterns map interpreted from the false color composite SPOT image of the study area (Original scale 1:20,000)

The main steps of image processing and interpretation for both the Landsat ETM+ and SPOT-5 data of the study area were conducted using the following methods:

- 1- Rectification and image enhancement of Landsat ETM+ and SPOT-5 data,
- 2- Unsupervised and supervised classification using SPOT-5 data,
- 3- Structural lineaments Extraction from SPOT-5 data, and
- 4- Detailed geological mapping of Kutaina-Al Hajar area.

3. Rectification and Image Enhancement of Landsat ETM+ and SPOT-5 Data

Raw digital satellite data usually includes geometric distortions due to the sensor geometry, the scanner, platform instabilities, the earth rotation, the earth curvature, etc., and it is necessary to correct for and adapt these distortions (Mather, 1987; Lillesand et al., 2004; Richards, 1995). The geometric correction is conducted for the digital data of the ETM+ bands of the study area using two main steps for image rectifications: rectification of a panchromatic ETM+ band 8 and rectification of the multispectral ETM+ bands (1 to 7). The correction in the first step occurred by collecting 185 well-distributed ground control points that were selected from the topographic sheets (scale 1:50,000) for the investigated area using the image to map method. The overall accuracy of the transformation is indicated by averaging the errors in the reference points and the root mean square error (RMS = 0.63, Bernstein, 1978). The cubic interpolation method is used in the resampling processing. The rectified panchromatic ETM+ band is then used as a geo-referenced base for the correction of the 6-multispectral ETM+ bands (1 to 7). In the second step, we used the image-to-image method. The geometric corrections of the SPOT-5 data were performed using the same methods.

The image enhancement procedure includes the production of a raw image that is more interpretable for a particular application (PCI Geomatica, 2003). The histogram equalization enhancement technique was applied to the ETM+ data from the study area to increase the contrast of the images (Schowengerdt 1983; Mather 1987; Lechi 1988). The enhanced false color composite Landsat ETM+ image (Fig. 2) for the study area was constructed from bands 7, 4 and 2, shown in red, green and blue, respectively, on a scale of 1:100,000. This image is used as a base map to construct the regional geological map of the investigated areas. The study area (Kutaina–Al Hajar) is delineated in Figure (2) by a yellow square.

The SPOT-5 digital data are used to construct large scale 1:20,000 images for the study area. The enhanced

false color composite SPOT image for Kutaina–Al Hajar area (Fig. 3) is a result of bands 4, 3 and 1, shown in red, green and blue, respectively, with an original scale of 1:20,000. This SPOT image is used as the base maps for tracing and constructing the detailed geological maps of the study area.

Figure (4) is a drainage pattern map of Kutaina–Al Hajar area, interpreted from the false color composite SPOT-5 image in Figure (3). This map shows the locations of both Kutaina mine and Al Hajar mine in the northern and southern parts respectively of the mapped area.

4. Unsupervised and Supervised Classification

Unsupervised classification is the procedures which carried out automatically by the computer, but the user enters the number of clusters and the distances between them. Figure 5 shows the results of the unsupervised classification of the digital SPOT-5 data which contains 8 classes expressing on 8 rock units of the study area. These classes are used as a base for helping in the training stage of supervised classification procedures.

Supervised classification is the procedures most often used for quantitative analysis of remote sensing image data. It rests upon using suitable algorithms to label the pixels in an image as representing particular ground cover types, or classes. A variety of algorithms is available for this, ranging from those based up on probability distribution models for the classes of interest to those in which the multispectral space is portioned into class-specific regions using optimally located surfaces, (Richards 1995).

Multispectral SPOT-5 digital data are used to perform the supervised classification and, indeed, the spectral pattern present within the data for each pixel is used as the numerical basis for categorization. That is, different features types manifest different combinations of DN's based on their inherent spectral reflectance and emittance properties. In the supervised classification the image analyst (supervises) the pixel categorization process by specifying, to the computer algorithm, numerical descriptors of the various land cover types present in a scene. Representative sample sites of known cover type, called training areas, are used to compile a numerical "interpretation key" that describes the spectral attributes for each feature type of interest. Each pixel in the data set is then compared numerically to each category in the interpretation key and labeled with the name of the category it "looks most like", (Lillesand et al. 2004).

The supervised classification is applied generally for the purpose of lithological discrimination, (Bischof et al. 1992 and Kanellopoulos et al. 1993). This study applied the supervised classification method using SPOT-5 data in the lithologic mapping of the Kutaina–Al Hajar area. The procedures of supervised classification method applied in this work including three main stages; Training stage, Classification Stage and Evaluation Stage.

4.1. Training stage

This is the first step of supervised classification method which needs a prior knowledge of the investigated area known as ground-truths. The computer should be feed by this information of ground truths in this stage. The information of ground truths are obtained and collected in this work from the Field

work and previous published geological maps of the investigated area.

The training data sets must be both representative and collected from all parts of the lithologic classes of the investigated area. This means that the image analyst must develop training statistics for all spectral classes constituting each information class to be discriminated by the classifier (Lillesand et al. 2004).

4.2. Classification stage

The classification stage is performed using software packages of remote sensing such as: Erdas Imagine, Geomatica PCI & Envi. They are usually containing some models of these classification methods such as Maximum Likelihood, Mahalanobis Distance and Minimum Distance. After performing the training stage in this work, the author chose the maximum Likelihood classifier method to apply on the SPOT-5 data of the study area using Erdas Imagine package. The maximum Likelihood classifier is one of the most known supervised classification method used in the geological mapping. This method depends on the probability of every pixel to be belongs to a specific class. The probability density functions are used to classify an unidentified pixel by computing the probability of the pixel value belonging to each category. Post classification smoothing method was applied in this work using the majority filter on the produced classified image to smooth it and gave a better classified map. Maximum Likelihood classifier method was applied and produced the supervised classified map of the study area (Fig. 6).

4.3. Evaluation stage

The evaluation of this supervised classification was carried out by comparing the supervised classified result map with ground truths reference data that are assumed to be true, in order to define the accuracy assessment of the classification and determine the

degree of acceptance. The overall accuracy is computed from the error matrix (Table-1) of classification (confusion matrix) by dividing the total number of correctly classified pixels (i.e., the sum of the elements along the major diagonal) on the total number of reference pixels. This analysis shows that the overall classification accuracy is good with 75 %. The Kappa coefficient is 0.75, so it could be accepted classification. Table (2) shows the Producers accuracy and users accuracy of this supervised classification. The highest value for both the Producers and users accuracy was 99 % for Wadi deposits. The lowest value for the Producers accuracy was 56 % for the altered metavolcanics, but its users accuracy was 78 %. The processed supervised classified thematic map was also correlated and checked in the field with the previous published geological maps.

Seven categories of the main lithologic units of the study area could be distinguished from the supervised classification map (Fig. 6). The altered metasediments bearing gold mineralizations in the study area are well recognized and delineated in this map and checked in the field (Fig. 7). The classified units are arranged from younger to older as follow:

- 1- Wadi Deposites: which are easily discriminated and delineated by the classified image map.
- 2- Granites: which are found mainly in the north western corner of the mapped area.
- 3- Altered Metavolcanics (MV): which are distributed mainly in the central and south eastern part of the mapped area.
- 4- Metavolcanics: which are found mainly in the eastern part of the mapped area (Fig. 8).
- 5- Altered Metasediments (MS): which are distributed in the central part of the mapped area.
- 6- Metasediments: which are found mainly in the western and south western parts of the mapped area (Figs. 9 & 10).

Table 1. Confusion (Error) matrix of the supervised classification

Class	Wadi Dep.	Pink Gr.	AltereMetav.	Metav.	AltereMetas.	Metas.	Total
Wadi Depos.	99.41	00.32	00.00	00.27	00.00	00.00	100
Pink Gran.	0.11	79.42	4.53	2.28	0.22	13.44	100
Altere Metav.	0.0	2.46	78.07	3.13	10.63	5.71	100
Metav.	0.00	1.76	3.79	88.32	5.30	0.53	100
Altere Metas.	0.30	2.25	42.32	10.67	37.91	6.85	100
Metas.	0.00	19.02	10.75	0.15	4.15	65.93	100
Total	99.82	105.23	139.46	104.82	58.21	92.46	600

$$\text{Overall accuracy} = 449.06 / 600 = 0.7484 = 75 \%$$

$$\text{KAPPA COEFFICIENT} = 0.7456 \text{ Standard Deviation} = 0.00139$$

Table 2. Producers accuracy and users accuracy of the supervised classification

Class	Producers Accuracy	Users Accuracy
Wadi Depos.	99.41 / 99.82 = 99 %	99.41 / 100 = 99 %
Pink Gran.	79.42 / 105.23 = 75 %	79.42 / 100 = 79 %
Altere Metav.	78.07 / 139.46 = 56 %	78.07 / 100 = 78 %
Metav.	88.32 / 104.82 = 84 %	88.32 / 100 = 88 %
Altere Metas.	37.91 / 58.21 = 65 %	37.91 / 100 = 38 %
Metas.	65.93 / 92.46 = 71 %	65.93 / 100 = 66 %

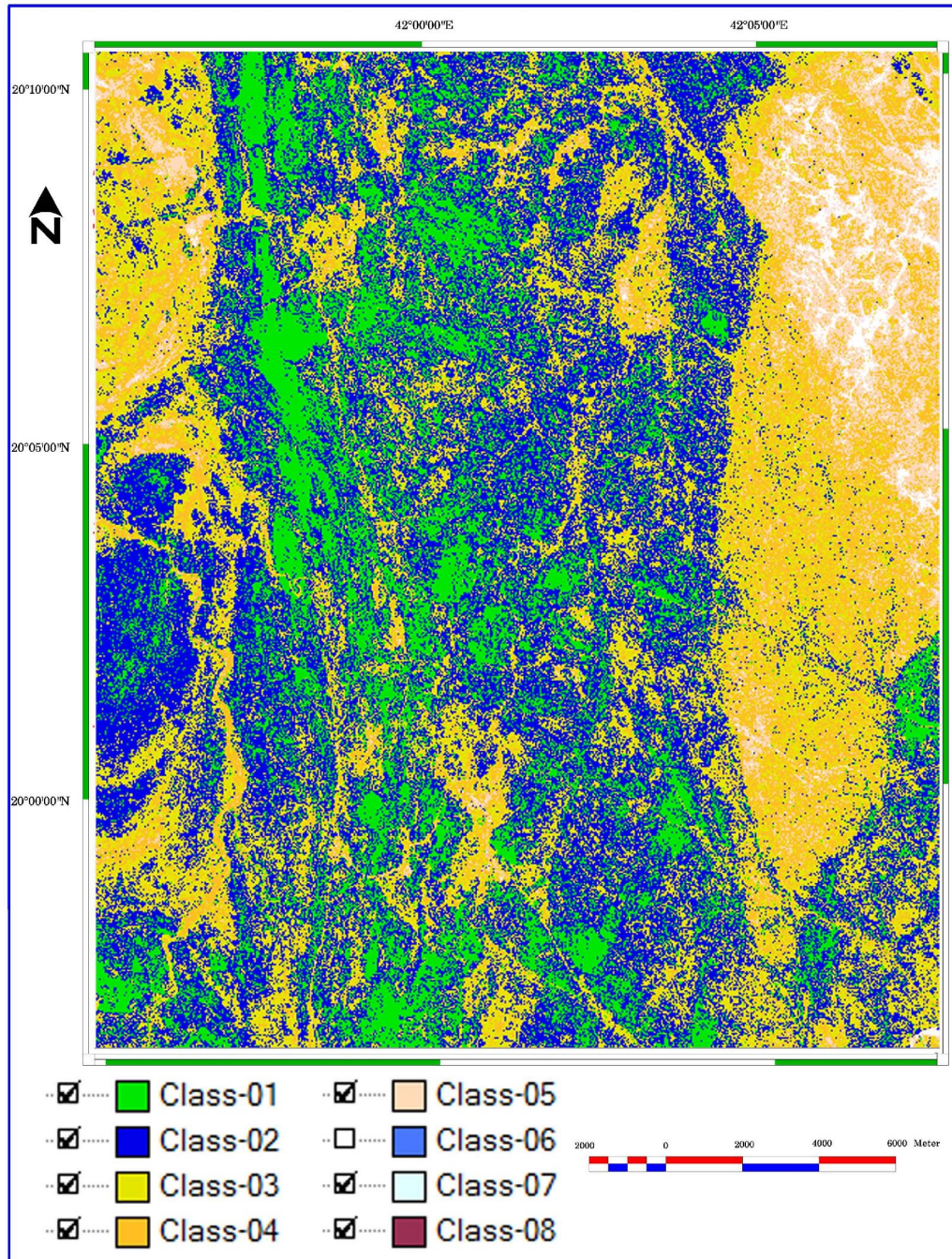


Figure 5. Unsupervised classification map of Kutaina–Al Hajar area (Original scale 1:20,000)

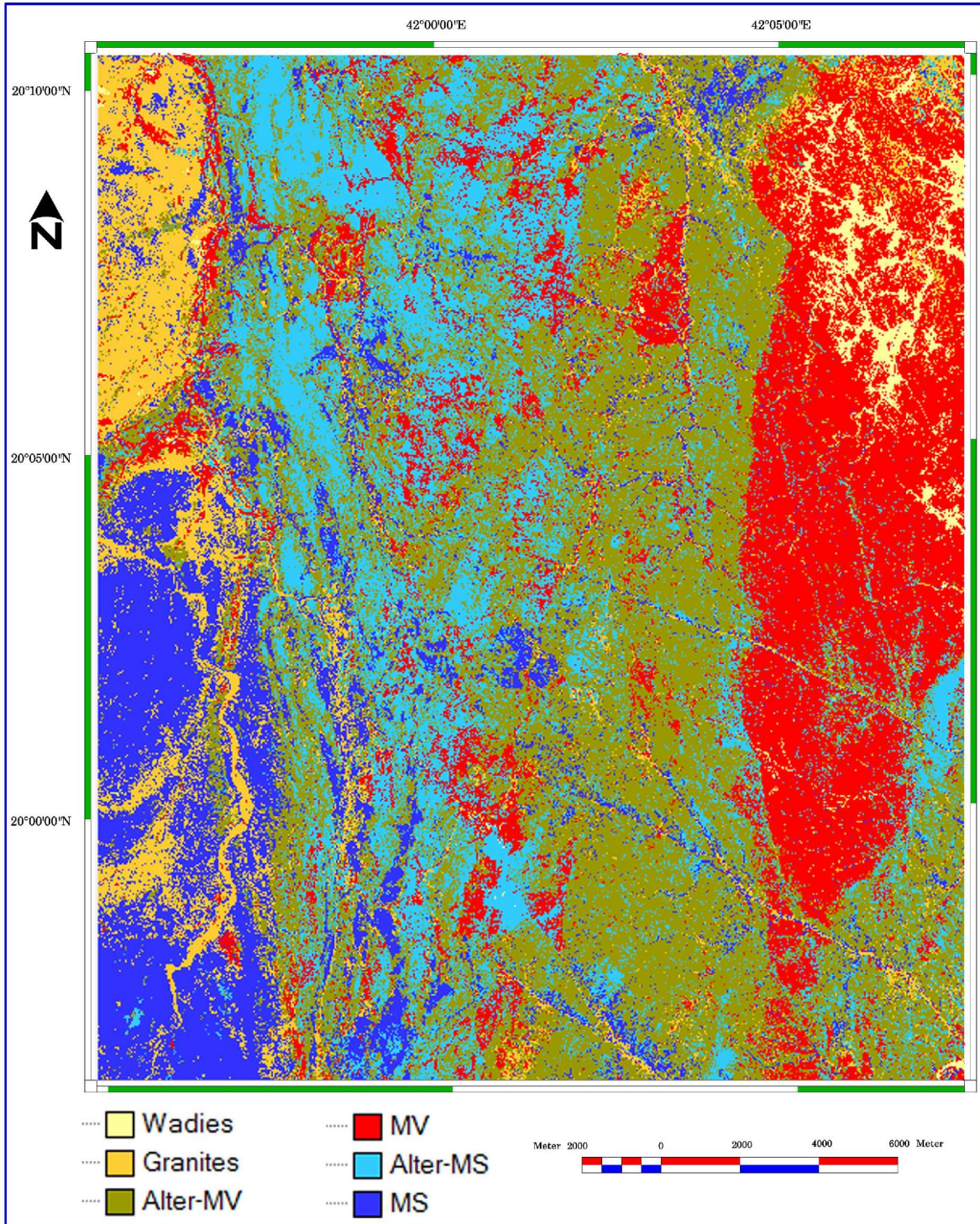


Figure 6. Supervised classification map of Kutaina–Al Hajar area (Original scale 1:20,000)

5. Structural Lineaments Extraction

Automatic lineaments extraction process was carried out using Geomatica PCI package and the digital remotely sensed data of SPOT-5 visible, NIR as well as the SWIR bands. The automatically lineaments extraction algorithm of Geomatica PCI

software consists of edge detection threshold and linear extraction steps. The steps of lineaments extraction have been done under the defined user parameters. Table 3 shows the difference between these parameters and the default parameters of the “Geomatica PCI” package.

The different multispectral SPOT-5 bands were tested to select the optimum band for the lineaments extraction. The relationship between SPOT-5 bands (wavelengths) and the number of the automatically extracted lineaments (frequency) for the study area is shown in Table 4. It has been noticed that the SWIR bands 3 and 4 exhibit the highest lineament number compared to the visible and NIR bands. The highest score of the lineaments number is recorded in band 4 (2310) whereas the lowest score of the lineaments number is recorded in visible band 2 (1320). Therefore, the automatically extracted lineaments using band 4 is used in this work for the structural lineaments interpretations.

The automatically extracted lineaments are visually edited to remove all the false lineaments which are not structurally controlled and adding any missed structural lineament. The obtained extracted structural lineaments patterns over SPOT-5 band-4 of the study area are shown in Figure 11 a. The statistical analyses of these significant structural lineaments have predominant trends in the NNW-SSE, NW-SE and WNW-ESE & NE-SW directions as shown in the rose diagram (Fig. 11 b). Comparing these structural trends of the investigated area as interpreted from the digital SPOT-5 data during this research with the previous literatures showed that, they are largely coincide with the main trends of the previous geological mapping.

6. Detailed geologic map

The detailed geological map of Kutaina-Al Hajar area is constructed in this work in a large scale 1:20,000, from the interpretation of the SPOT-5 images and the supervised classified image, which showing in Figure (12). This map shows the main lithologic units of the investigated area arranged from youngest to the oldest, Wadi deposits, granitic rocks, altered metavolcanics, metavolcanics, altered metasediments and metasediments.

Figure 12, shows a new detailed geological map of Kutaina-Al Hajar area, scale 1 : 20,000, which was mainly generated from applying image processing of SPOT-5 data and the field verifications. The main seven lithostratigraphic units of the investigated area is interpreted mainly from the supervised classification image (Fig. 6). This supervised classified image was greatly improved and supplemented by the results of the FCC image (Fig. 3). The lithologic interpretations of figures 3 and 6 and the structural interpretations of Figures 11 and in addition to the drainage base map (Fig. 2) and field verifications, gave rise to the new detailed geological map of Kutaina-Al Hajar area in a large scale 1:20,000 (Fig. 12). This geological map showing the main regional faults which cutting the investigated area in

the predominant NW-SE and NNW-SSE trends, as well as the interpreted dikes, antiform, synform, joints and fractures.

Table 3: Default and user parameters used for automatic extraction of lineaments in PCI Package

PCI Parameters	Default Values	User Values
Edge filter radius	3 (Pixels)	3 (pixels)
Minimum edge gradieny	15 (Pixels)	15 (Pixels)
Minimum line length	15 (Pixels)	10 (Pixels)
Line fitting tolerance	2 (Pixels)	10 (Pixels)
Maximum angular difference	10 (Degree)	30 (Degree)
Maximum linking difference	30 (Pixels)	60 (Pixels)

Table 4. SPOT-5 multispectral bands versus the extracted lineaments frequency for Kutaina –Al Hajar area

SPOT-5 bands	Lineaments (Frequency)
Band-1	1510
Band-2	1320
Band-3	1950
Band-4	2310



Figure 7. Field photograph showing the altered metasediments, in the open pit, Al Hajar mine, looking S



Figure 8. Field photograph showing the metasediments and metavolcanics, in Kuation-Al Hajar area, looking N E.



Figure 9. Field photograph showing shear-sense indicator in the foliation planes of the metasediments, looking E.



Figure 10. Field photograph showing a panoramic view of the altered metasediments, in Kutaina–Al Hajar area, looking N

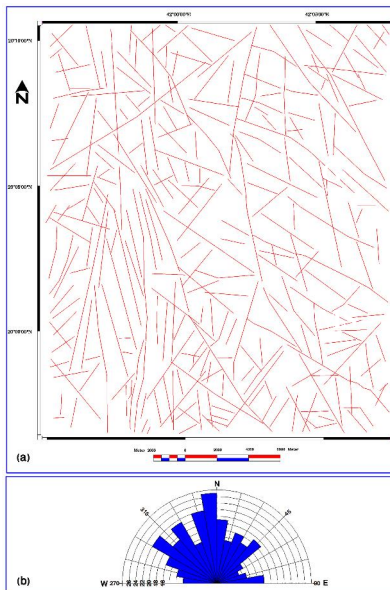


Figure 11. (a) Structural lineaments extracted from the false color SPOT image, (b) Rose diagram showing the main trends of the extracted structural lineaments

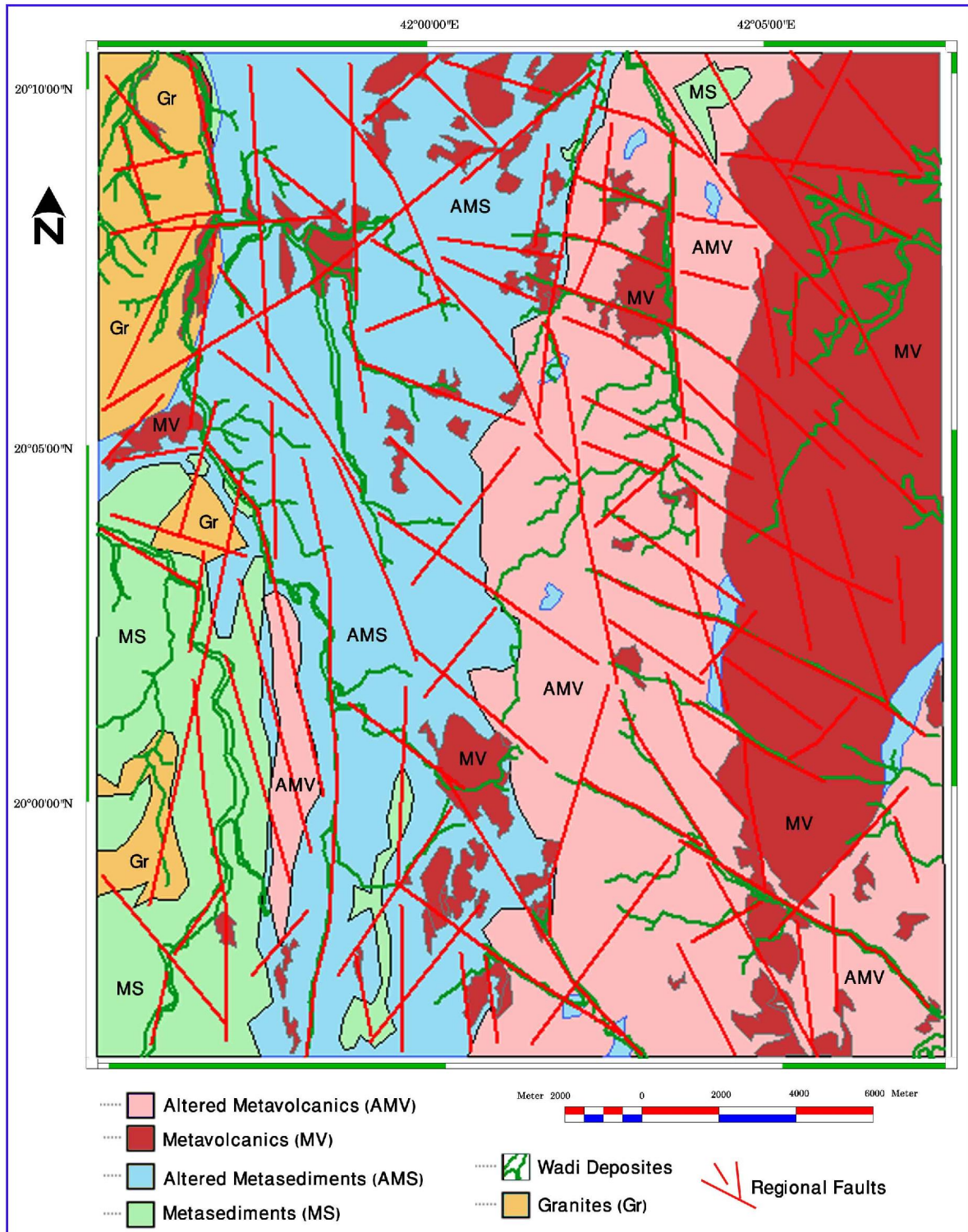


Figure 12. Geological map of Kutaina–Al Hajar area (Original scale 1:20,000)

7. Conclusions

The lithological units and the structural element framework of the study area were mapped in detail during this study on a scale of 1:20,000. A detailed analysis of the processed Landsat ETM+ and SPOT-5 imagery was performed by mapping the studied areas.

The color signatures of some rock units are easily recognized and visually interpreted on the color composite Landsat and SPOT images. The rock units primarily include porphyry granitic rocks, metavolcanics, altered, metavolcanics, metasediments, and altered metasediments. This study revealed the following conclusions:

- Kutaina-Al-Hajar area is located in Asir terrane in the south central part of the Arabian Shield. It is covered by Precambrian metasediments and metavolcanics of low-grade green-schist facies rocks. They are intruded by many igneous plutonic bodies.

-Different image processing techniques, such as image enhancement, color composite images, multispectral classification, and structural lineaments extraction are applied in this work for the lithological and structural discrimination of the investigated area.

- The processed Landsat color composite and the SPOT-5 color composite images assisted in providing more lithological and structural information for the study area. The new detailed geological map of the investigated area on a large scale of 1:20,000 was constructed using the constructed SPOT-5 classified images. The constructed new geological map of the study area was verified in the field. It is recommended to apply the different image processing techniques with high spectral and spatially resolution satellite digital data for detailed geological mapping.

- The host rocks of the mineralization are green-schist facies with metasediments and metavolcanic rocks of Pre-Cambrian age.

- This study revealed that the alteration zones in Kutaina - Al Hajar area are mainly associated with the altered metasediments and altered metavolcanics rocks. The mineralized zones in the investigated area are also controlled by the structural trends in the N-S, NW-SE, WNW-ESE and NE-SW directions, that were recognized and analyzed during this study.

Correspondence to:

Prof. Adel Zein Bishta
Faculty of Earth Sciences, King Abdulaziz University,
Jeddah, P.O. Box: 80206 Jeddah: 21589, Saudi Arabia
Telephone: +966530911301
Emails: abishta@kau.edu.sa or
adel_zein2@yahoo.com

References

1. Abrams MJ, Brown D, Lepley L, Sadowski R. Remote sensing for porphyry copper deposits in southern Arizona. *Economic Geology* 1983; 185 (78): 591–604.
2. Al-Shanti AMA. *Geology of the Arabian Shield of Saudi Arabia*. Scientific Publishing Centre, King Abdulaziz University, 2009; 1st ed., 190p. Jeddah.
3. Amer R, Kusky T, Ghulam A. Lithological mapping in the Central Eastern Desert of Egypt using ASTER data. *Journal of African Earth Sciences* 2009; 56 (2):75-82. DOI: 10.1016/j.jafrearsci.2009.06.004.
4. Antonielli B, Fidolini F, Righini G. Landsat TM and Quickbird images for geological mapping in the syn-rift Lower Dogali Formation (Red Sea coast, NE Eritrea). *PHOTO INTERPRETATION* 2009; 3: 107-114.
5. Bamousa AO. Infracambrian superimposed tectonics in the Late Proterozoic units of Mount Ablah area, southern Asir terrane, Arabian Shield, Saudi Arabia. *Arab Journal of Geosciences* 2013; 6: 2035-2044.
6. Bernstein R. *Digital image processing for remote sensing*, IEEE press 1978.
7. Bishta AZ. Lithologic discrimination of Gabal Qattar-Um Disi environs, North Eastern Desert of Egypt using thematic mapper data of Landsat-7. *The third International Symposium on Geophysics*, Tanta University, Tanta, Egypt, 2004; 541-557.
8. Bishta A Z. Lithologic discrimination using selective image processing techniques of Landsat-7 data, Um Bogma environs, West central Sinai, Egypt. *Journal of King Abdulaziz University (JKAU): Earth Sciences* 2008; 21:193-213.
9. Bishta A Z. Assessing utilization of multi-resolution Satellite imageries in geological mapping, a case study of Jabal Bani Malik area, eastern Jeddah city, Kingdom of Saudi Arabia. *Journal of King Abdulaziz University (JKAU): Earth Sci.* 2010; 21 (1) 27-52.
10. Blenkinsop TG, Doyle, MG. Structural controls on gold mineralization on the margin of the Yilgarn craton, Albany-Fraser orogen: The Tropicana deposit, Western Australia. *Journal of Structural Geology* 2014; 67: 189-204.
11. Davis PA, Berlin GL. Rock discrimination in the complex geological environment of Jabal Salma, Saudi Arabia using Landsat Thematic Mapper data. *Photogrammetric Engineering & Remote Sensing* 1989; 7: 1147-1160.

12. Deksissa DJ, Koeberl C. Geochemistry, alteration, and genesis of gold mineralization in the Okote area, southern Ethiopia. *Geochemical Journal* 2004; 38:307-331.
13. Doyle MG, Fletcher IR, Foster J, Large RR, Mathur R, McNaughton NJ, Meffre S, Muhling JR, Phillips D, Rasmussen B. Geochronological Constraints on the Tropicana Gold Deposit and Albany-Fraser Orogen, Western Australia. *Economic Geology* 2013; 110: 355-386.
14. El Janati M, Soulaïmani A, Admou H, Youbi N, Hafid A, Hefferan KP. Application of ASTER remote sensing data to geological mapping of basement domains in arid regions: a case study from the Central Anti-Atlas, Iguerda inlier, Morocco. *Arabian Journal of Geosciences* 2013; 7 (6): 2407-2422.
15. Gibson J, Power CH. *Introductory remote sensing digital image processing and application*. London: Routledge 2000.
16. Guha A, Kumar KV, Rao EN, Parveen R. An image processing approach for converging ASTER-derived spectral maps for mapping Kolhan limestone, Jharkhand, India. *Current Science* 2014; 106 (1): 40-49.
17. Gupta RP. *Remote sensing geology*. Springer, Berlin 2003, 2nd ed., 656 p.
18. Haselwimmer CE, Riley TR, Liu JG. Assessing the potential of multispectral remote sensing for lithological mapping on the Antarctic Peninsula: case study from eastern Adelaide Island, Graham Land. *Antarctic Science* 2010; 22 (3): 299–318.
19. Jutz SL, and Chorowicz J. Geological mapping and detection of oblique extension structures in the Kenyan Rift Valley with a SPOT/Landsat-TM datamerge. *International Journal of Remote Sensing* 1993; 14: 1677-1688.
20. Kavak KS, Cetin H. A Detailed Geologic Lineament Analysis Using Landsat TM Data of Golmarmara/Manisa Region, Turkey. *Online Journal of Earth Sciences* 2007; 1: 145-153. doi:ojesci.2007.145.153.
21. Lechi G. Satellite sensors and satellite image characteristic. Rep 11th international training course on applications of remote sensing to agricultural statistics (5-20 May 1986), Remote and Montpellier FAO, Rome 1988.
22. Lillesand TM, Kiefer RW, Chipman JW. *Remote sensing and image interpretation* 2004; 4th ed., John Wiley and Sons Inc. New York, ISBN: 0-471-25515-7, 763 p.
23. Madani A, Bishta AZ. Selection of the optimum bands of Landsat 7 ETM+ for automatic lineaments extraction: A case study of Gattar Granites, North Eastern Desert, Egypt. *Geology of the Arab World*, Cairo University 2002; 6: 323-360.
24. Mather PM. *Computer processing of remotely sensed images, an introduction* 1987; John Wiley and Sons, ISBN: 0 – 471 – 9064 –4.
25. PCI Geomatica. *Software helps* 2003; 9.1.
26. Richards JA. *Remote sensing, digital image processing, an introduction* 1995; Springer-Verlag New York, Inc. Secaucus, NJ, USA. ISBN: 0387548408.
27. Sabins FF. Remote sensing for mineral exploration. *Ore Geology Reviews* 1999; 14: 157–183.
28. Schowengerdt RA. *Techniques for image processing and classification in remote sensing*. Academic Press, Inc., US, 1983; ISBN: 0 – 12-62890 – 8.
29. Sultan M, Arvidson RE, Sturchio NC. Mapping of serpentinites in the Eastern Desert of Egypt by using Landsat Thematic Mapper data. *Geology* 1986; 14: 995-999. Available at: <http://glovis.usgs.gov>.
30. Sultan M, Arvidson RE, Sturchio NC, Guinness EA. Lithologic mapping in arid regions with Landsat thematic mapper data: Meatiq dome, Egypt. *Geological Society of America Bulletin* 1987; 99: 748-762.
31. Wielen VS, Oliver S, Kalinowski A. Remote sensing and spectral investigations in the western succession, mount Isa Inlier, implications for exploration. *Predictive mineral discovery CRC Conference* 2004, Barossa Valley 1-3 June 2004.